Lab on a Chip

Contact Photolithography-Free Integration of Patterned and Semi-Transparent Indium Tin Oxide Stimulation Electrodes into Polydimethylsiloxane-Based Heart-on-a-Chip Devices for Streamlining Physiological Recordings

Journal:	*Lab on a Chip*
Manuscript ID	LC-ART-09-2020-000948.R1
Article Type:	Paper
Date Submitted by the Author:	26-Nov-2020

Complete List of Authors:	Yip, Joycelyn; University of Southern California Viterbi School of Engineering, Department of Biomedical Engineering Sarkar, Debarghya; University of Southern California Viterbi School of Engineering, Department of Electrical Engineering Petersen, Andrew; University of Southern California Viterbi School of Engineering, Department of Biomedical Engineering Gipson, Jennifer; University of Southern California Viterbi School of Engineering, Department of Biomedical Engineering Tao, Jun; University of Southern California Viterbi School of Engineering, Department of Electrical Engineering Kale, Salil; University of Southern California Viterbi School of Engineering, Department of Electrical Engineering Rexius-Hall, Megan; University of Southern California Viterbi School of Engineering, Department of Biomedical Engineering Cho, Nathan; University of Southern California, Biomedical Engineering Khalil, Natalie; University of Southern California Viterbi School of Engineering, Department of Biomedical Engineering Kapadia, Rehan Rashid; University of Southern California Viterbi School of Engineering, Department of Biomedical Engineering McCain, Megan; University of Southern California, Biomedical Engineering; USC

Full Title

Contact Photolithography-Free Integration of Patterned and Semi-Transparent Indium Tin Oxide Stimulation Electrodes into Polydimethylsiloxane-Based Heart-on-a-Chip Devices for Streamlining Physiological Recordings

Authors

Joycelyn K. Yip, [a†] Debarghya Sarkar, [b†] Andrew P. Petersen,[a] Jennifer Gipson,[a] Jun Tao,[b] Salil Kale,[b] Megan L. Rexius-Hall,[a] Nathan Cho,[a] Natalie N. Khalil,[a] Rehan Kapadia,*[b] and Megan L. McCain*[ac]

Affiliations

[a]Laboratory for Living Systems Engineering, Department of Biomedical Engineering, USC Viterbi School of Engineering, University of Southern California, Los Angeles, CA 90089.

[b]Ming Hsieh Department of Electrical Engineering, USC Viterbi School of Engineering, University of Southern California, Los Angeles, CA 90089.

[c]Department of Stem Cell Biology and Regenerative Medicine, Keck School of Medicine of USC, University of Southern California, Los Angeles, CA 90033.

† These authors contributed equally to this work.

* Co-Corresponding Authors:

Megan L. McCain
mlmccain@usc.edu

Rehan Kapadia
rkapadia@usc.edu

Abstract

Controlled electrical stimulation is essential for evaluating the physiology of cardiac tissues engineered in Heart-on-a-Chip devices. However, existing stimulation techniques, such as external platinum electrodes or opaque microelectrode arrays patterned on glass substrates, have limited throughput, reproducibility, or compatibility with other desirable features of Heart-on-a-Chip systems, such as the use of tunable culture substrates, imaging accessibility, or enclosure in a microfluidic device. In this study, indium tin oxide (ITO), a conductive, semi-transparent, and biocompatible material, was deposited onto glass and polydimethylsiloxane (PDMS)-coated coverslips as parallel or point stimulation electrodes using laser-cut tape masks. ITO caused substrate discoloration but did not prevent brightfield imaging. ITO-patterned substrates were microcontact printed with arrayed lines of fibronectin and seeded with neonatal rat ventricular myocytes, which assembled into aligned cardiac tissues. ITO deposited as parallel or point electrodes was connected to an external stimulator and used to successfully stimulate micropatterned cardiac tissues to generate calcium transients or propagating calcium waves, respectively. ITO electrodes were also integrated into the cantilever-based muscular thin film (MTF) assay to stimulate and quantify the contraction of micropatterned cardiac tissues. To demonstrate the potential for multiple ITO electrodes to be integrated into larger, multiplexed systems, two sets of ITO electrodes were deposited onto a single substrate and used to stimulate the contraction of distinct micropatterned cardiac tissues independently. Collectively, these approaches for integrating ITO electrodes into Heart-on-a-Chip devices are relatively facile, modular, and scalable and could have diverse applications in microphysiological systems of excitable tissues.

Introduction

In recent years, microphysiological systems and Organs-on-Chips have emerged as valuable *in vitro* models for human disease modeling[1] and drug discovery.[2, 3] These are microfabricated systems designed to engineer cells into microscale tissue constructs that mimic key biological, chemical, and/or physical features of native tissues and efficiently provide physiologically-relevant, quantitative readouts in a scalable manner.[4, 5] Heart-on-a-Chip systems have focused on modeling the myocardium, which is comprised of layers of cardiac myocytes organized into parallel fiber-like structures and embedded in a compliant extracellular matrix to maximize electrical signal propagation, uniaxial force generation, and cardiac output.[6] To mimic physical features of native myocardium *in vitro*, cardiac myocytes are routinely cultured on substrates with tunable rigidity, such as polydimethylsiloxane (PDMS)[7-9] or hydrogels,[10-12] that are micropatterned using microcontact printing of extracellular matrix proteins[13, 14] or topographical features[11, 15, 16] to induce cell alignment. In parallel, several functional assays have been developed to quantify functional outputs related to electrophysiology and tissue contractility *in vitro*. For example, the morphology and propagation of action potentials and calcium transients can be optically imaged in engineered cardiac tissues with voltage- and calcium-sensitive dyes[13, 17-20] or genetically-encoded sensors[21-23]. To measure contractile stresses, assays such as the cantilever-based muscular thin film (MTF) assay[11, 13, 24-26] and traction force microscopy[12, 27-29] are often implemented for two-dimensional cardiac tissues. However, a relatively ubiquitous technical hurdle for these functional assays is the requirement for user-defined electrical stimulation at specific locations, frequencies, and voltages.

Conventional strategies for electrically stimulating cardiac tissues *in vitro* impose constraints on throughput, reproducibility, and integration of other desirable features of Heart-on-a-Chip systems, such as use of tunable culture substrates, imaging accessibility, or

enclosure in a microfluidic device. For example, global or local electrical stimulation is often applied by manually positioning parallel or point electrodes, respectively, fabricated from platinum or other corrosion-resistant metals in the bath above a tissue.[9, 12-14, 26] This approach is time-intensive and low-throughput, has poor reproducibility and low spatial resolution, and is incompatible with tissues enclosed in microfluidic devices, which are increasingly implemented for microphysiological systems to increase throughput and automate the delivery and exchange of media and other soluble factors between tissues. Wire electrodes have also been embedded into culture chambers,[30-34] which increases throughput and compatibility with enclosed devices, but is still limited by poor spatial resolution. To increase spatial resolution and reproducibility, photolithography has been used to pattern metals such as titanium nitride,[35-39] palladium,[40] aluminum,[41] and gold[42] into microelectrode arrays adhered directly onto glass substrates used for cell culture. However, contact photolithography is incompatible with rapid prototyping, which slows device fabrication and the iterative design process. Conventional metals used for microelectrode arrays are also not optically transparent and thus obstruct live cell imaging. Another limitation is the use of glass substrates, which precludes the integration of many of the tunable biomaterials, surface engineering techniques, and assays described above that are a priority for Heart-on-a-Chip systems. Although gold electrodes have been fabricated on PDMS,[43-45] this approach is still not ideal due to the reliance on photolithography and the opacity of the gold electrodes.

Indium tin oxide (ITO) is one of the most widely utilized transparent conductive oxide thin films for solar cells,[46, 47] photodetectors,[48-50] and displays[51, 52] due to its favorable electrical and optical properties. ITO is also a promising material for biosensor and biotechnology applications due to its high conductivity, substrate adhesion, stability in electrolyte-rich solutions, relatively low cost, and optical transparency. ITO films on glass slides are cytocompatible[53] and have been implemented for cell electroporation,[54, 55] cell lysis,[56] cellular impedance measurements,[57, 58] and stimulation[59] and recording[60] of

extracellular potentials in neurons. ITO-coated glass slides have also been laser ablated to create custom electrode arrays to electrically stimulate cardiac myocytes.[61] However, patterned ITO electrodes have not been integrated into Heart-on-a-Chip systems that offer additional features, such as tunable culture surfaces and sophisticated physiological assays.

In this study, we implemented laser-cut tape masks to pattern ITO as parallel or point electrodes onto culture substrates as a facile and higher throughput alternative to photolithography that still affords the spatial resolution required for tissue-level Heart-on-a-Chip assays. Depending on the assay of interest, ITO electrodes were patterned directly on glass or PDMS, the latter of which was then microcontact printed with fibronectin prior to seeding with neonatal rat cardiac myocytes. This resulted in the formation of aligned myocardial tissues adhered to a relatively compliant surface integrated with semi-transparent parallel or point electrodes that did not interfere with routine brightfield microscopy. We then implemented the patterned ITO electrodes to stimulate engineered cardiac tissues either globally or locally to quantify calcium transient morphology, propagation velocity, and contractility using existing Heart-on-a-Chip assays. We also patterned two sets of ITO electrodes with corresponding arrays of MTFs on the same substrate and simultaneously paced the MTF arrays at distinct frequencies, demonstrating the potential for patterned ITO electrodes to be leveraged in multiplexed platforms that also provide sophisticated functional readouts. Together, these results demonstrate that our photolithography-free, facile approach for patterning semi-transparent ITO electrodes on both glass and PDMS is relatively modular and easy to integrate with existing Heart-on-a-Chip substrates and assays, which can be extended to improve the usability and scalability of microphysiological systems for many types of excitable tissues.

Experimental

Mask fabrication

Patterns for each layer of the device (ITO, PDMS, PIPAAm) were designed in CorelDRAW X7 (Corel Corporation, Ottawa, Canada), as shown in Fig. S1. Low-adhesion tape (3900R CLR360 Embossed Removable Protective Film Tape, Patco, Maspeth, NY, USA) was attached onto a metal plate and cut into masks with a non-contact, 40 W CO_2 laser in an Epilog Mini 18 (Epilog Laser, Golden, CO, USA) at 18% speed, 6% power, and 2500 Hz. The negative areas intended for material deposition were peeled away using tweezers, as shown in Fig. S2. Tape masks were then transferred and aligned on top of clean glass coverslips (22 mm × 22 mm × 0.19-0.25 mm).

Material deposition

For versions of the device designated for calcium imaging, coverslips were first spin-coated with PDMS without tape masks, then layered with ITO following the masking and deposition protocols described below. For the MTF version of the device, ITO was deposited first on glass coverslips, then layered with PIPAAm and PDMS. Detailed photographs of the fabrication process are provided in Fig. S2.

For ITO deposition, bare or PDMS-coated glass coverslips masked with parallel or point electrode designs (Fig. S1A and Bi) were secured on top of a silicon wafer with heat resistant tape (Kapton Tape, Hxtape, Dongguan, China). The silicon carrier wafer with samples was attached to a chuck and loaded in an ultra-high vacuum chamber (Kurt J. Lesker Company, Jefferson Hills, PA, USA) with a base pressure < 1e-6 torr for ITO deposition. ITO was radio frequency sputtered at a deposition pressure of 3 mTorr Argon and 48 W power for 80 min to produce a 200 nm thick film. The ITO target used was 2” diameter 99.99% pure In_2O_3:SnO_2, 90:10 wt % elastomer-bonded assembly (TORUS Mag Keeper, Kurt J. Lesker

Company, Jefferson Hills, PA, USA). After deposition, the tape masks were removed and the conductivity of the ITO on the coverslips was validated using a handheld multimeter.

For PIPAAm deposition, tape masks (Fig. S1Bii) were placed on top of ITO-covered coverslips. 10% (wt:vol) solution of PIPAAm (Polysciences, Warrington, PA, USA) in 99% butanol was spin-coated on top of each masked coverslip, as previously described.[13, 24-26] Tape masks were carefully peeled away to preserve the PIPAAm layer.

For PDMS deposition, bare or masked (Fig. S1Biii) coverslips were spin-coated with a layer of PDMS (10:1 (wt:wt) Sylgard 184; Dow Corning Corporation, Midland, MI, USA) and cured at 65 °C. After 4 hours of incubation, masks were carefully removed using tweezers. For MTF substrates, cantilever outlines were laser-cut into the PDMS and PIPAAm layers at 17% speed, 4% power, and 2500 Hz, as previously described.[26] The cantilevers were 3 mm × 1.5 mm, spaced 0.65 mm apart.

ITO electrical characterization

Resistance of the surface of substrates was measured by the standard four-point probe measurement. Assuming the current flow to be uniform across the entire thickness of the film, the thickness-normalized resistance or sheet resistance of the film is calculated as $R_s = R \times W L^{-1}$, where W is the width of the electrodes and L is the length between the electrodes.

ITO optical characterization:

Transmittance of the substrates was measured using a custom-built optical measurement setup. A broadband white-light source (SLS201L, Thorlabs, Newton, NJ, USA) was used for the excitation, and the transmitted spectrum was obtained on a spectrometer (CCS200, Thorlabs, Newton, NJ, USA).

Multiphysics modeling

Electric field profiles were simulated by finite element methods in the Current Flow environment of Finite Element Method Magnetics software (FEMM Version 4.2, femm.info). Relative permittivity of ITO was chosen as 3.33,[62] while that of the culture media was chosen as 80.[63] Conductivity of the media was taken as 1.5 S m^{-1},[63] while that of 200 nm ITO was taken as 1.6e4 S m^{-1} from experimental values of sheet resistance, assuming uniform current conduction throughout the ITO thin film. For the external platinum wire parallel electrode simulations, the conductors were assumed to be perfect due to the extremely high conductivity of platinum relative to the culture media (1e7 S m^{-1} to 1.5 S m^{-1}, respectively). The distance between the electrodes was 12 mm, which is representative of these types of electrodes.

Stamp fabrication and microcontact printing of fibronectin

Standard photolithography and soft lithography techniques were used to fabricate master wafers and PDMS stamps.[64] Briefly, a silicon wafer was spin-coated with a layer of negative photoresist (SU-8 2002; MicroChem Corp., Newton, MA, USA) and positioned with a photolithographic mask with 15 μm wide lines separated by 2 μm gaps using a standard mask aligner (MJB3 Contact Aligner, SÜSS MicroTec, Garching, Germany). The masked wafer was exposed to high-energy UV light, baked, and immersed in developer solution to remove unexposed photoresist. The wafer was then silanized with trichloro(1H, 1H, 2H, 2H-perfluorooctyl)silane overnight in a vacuum desiccator. PDMS was then poured on top of the master wafer in 150 mm dishes and degassed again at 70 mmHg to remove residual air bubbles. After curing at 65 °C for at least 4 h, the PDMS piece was cut into individual PDMS stamps measuring 22 mm × 22 mm, the same dimensions as the glass coverslips.

Following previously published protocols,[7, 9, 12, 13, 24-26] PDMS stamps were sonicated in 95% ethanol and dried using compressed air in a sterilized biosafety cabinet. Human

fibronectin in distilled, deionized water (50 ug mL^{-1}, Corning Inc., Corning, NY, USA) was pipetted onto the surface of each stamp and incubated for 1 h at room temperature. ITO-coated coverslips were treated in a UVO cleaner (Model 342, Jelight Company Inc., Irvine, CA, USA) for 8 min to sterilize and oxidize the surface. Stamps were then dried under compressed air, inverted gently onto treated coverslips to transfer the fibronectin, and carefully removed. The coverslips remained in a sterile hood until chamber attachment and seeding.

PDMS chamber design and bonding

All chambers were designed in SolidWorks 2018 CAD Package (Dassault Systèmes SolidWorks Corporation, Waltham, MA, USA), as seen in Fig. S3. For the contractility device, the multi-well PDMS chamber consists of a 6.5 mm surrounding wall with a 3.5 mm divider splitting the chamber into two equally sized compartments. The inverse of this chamber, with extensions along the length to ease removal, was extruded in plastic with a desktop three-dimensional printer (MakerBot Replicator 2, MakerBot Industries LLC, Brooklyn, NY, USA). This was then used as a template for molding chambers of PDMS cured in the same process as described above. After removal, each chamber was trimmed to a length of 22 mm. Chambers were sterilized and oxidized in a UVO cleaner, coated with uncured PDMS on the bottom, and centered on top of coverslips in alignment with the electrode pattern. The devices were cured overnight in a sterile hood. For the calcium imaging device, PDMS chambers without the divider were attached in the same manner.

Cardiac myocyte harvest, seeding, and culture

Neonatal rat ventricular myocytes were isolated from two-day-old neonatal Sprague-Dawley rats, as previously described.[7, 9, 12, 13, 24-26] Isolation was performed according to protocols approved by the University of Southern California Institutional Animal Care and Use

Committee, protocol 20133. Ventricles were harvested, cut into 2-5 mm pieces, and incubated in trypsin solution (1 mg mL^{-1}, Affymetrix, Santa Clara, CA, USA) in Hanks' balanced salt solution for 11-13 h at 4 °C. Ventricles were further digested into a single-cell suspension with four collagenase (1 mg mL^{-1}, Worthington Biochemical) triturations for 2 min each at 37 °C, followed by manual pipette agitation. Cells were then strained, resuspended in M199 culture medium supplemented with 10% heat-inactivated FBS, 10 mM HEPES, 0.1 mM MEM nonessential amino acids, 20 mM glucose, 2 mM L-glutamine, 1.5 μM vitamin B-12, and 50 U mL^{-1} penicillin. The cells were preplated twice to minimize the population of non-cardiac myocytes. Each device was seeded with 750,000 cells and incubated at 37 °C overnight. Devices were then washed twice with PBS and incubated in fresh culture medium with 10% FBS. After two days, the FBS concentration was reduced to 2% in order to reduce fibroblast proliferation. Cells were cultured for three days prior to conducting experiments.

Calcium imaging and analysis

Similar to previous studies,[9, 17, 19] devices were incubated with 1.7 ug mL^{-1} Fluo-4 AM (Life Technologies, Carlsbad, CA, USA) for 30 min, immersed in Tyrode's solution, and moved to the stage of an inverted fluorescent microscope (Nikon Eclipse Ti, Nikon Corporation, Tokyo, Japan) enclosed in a 37 °C incubation chamber (OKOLAB USA Inc., San Bruno, CA, USA). The ITO electrode was connected to an external stimulator (Myopacer, IonOptix, Westwood, MA, USA) using conductive tape. Image sequences (4 s) of the calcium transient fluorescence were captured at 20 V at 0.5, 1.0, and 2.0 Hz using a 2x air objective and a high-speed camera (Andor Zyla sCMOS, Oxford Instruments, Abingdon, UK) at 100 frames per second, 4 × 4 binning, and a gain of 4.

Calcium transients were extracted by plotting average fluorescence intensity of a specified region of interest and processed using custom MATLAB software (MATLAB, MathWorks, Natick, MA, USA). Calcium wave propagation velocity was also calculated

using custom MATLAB software, as previously described.[9, 19] Briefly, the recorded image sequence was divided into individual activation cycles based on the stimulation frequency. For every pixel in each activation cycle, the activation threshold was calculated using the mean and standard deviation of the fluorescence intensity. When the fluorescence intensity of the pixel exceeded the activation threshold, an activation time was recorded. The activation times of each pixel were plotted into a two-dimensional heat map that displays the wave of calcium release across the tissue. Specified regions of interest were manually selected in the direction of tissue alignment and the x-position (mm) of each pixel was plotted against its respective activation time (s). Calcium wave propagation velocity was defined as the slope of the line (cm s^{-1}) after robust linear regression.

MTF contractility assay and analysis

MTF devices were rinsed in Tyrode's buffer solution (0.5 mM HEPES, 0.1 mM magnesium chloride, 0.54 mM potassium chloride, 0.33 mM sodium phosphate, 1.8 mM calcium chloride, 5.0 mM glucose, pH 7.4 at 37 °C) and placed on the stage of a stereomicroscope. The temperature of the solution was decreased to room temperature to allow the phase transition of PIPAAm to liquid. Tweezers were used to manually peel each MTF away from the coverslip as the PIPAAm layer dissolved. When all films were peeled, the devices were refilled with 37 °C Tyrode's. Each pair of electrodes were connected to external field stimulators (Myopacer, IonOptix, Westwood, MA, USA) using conductive tape. The films were paced at 0.5, 1.0, and 2.0 Hz, and their movement was recorded from above at 100 frames per second. The stimulation voltage was set at 20 V. Each set of films was also paced at different frequencies using two separate stimulators.

The longitudinal planar projections of contracting MTFs were automatically detected using custom ImageJ software (National Institutes of Health, Bethesda, MD, USA) and used to derive the radius of curvature using custom MATLAB code (Mathworks, Natick, MA,

USA), as previously described.[13, 25] Radius of curvature, elastic modulus, and thickness of the MTFs was used to calculate the stress generated using previously published models.[13, 25]

Due to the limited field of view of the stereomicroscope, a cell phone (iPhone 8, Apple Inc., Cupertino, CA, USA) was used to record the entirety of the device from above for multiplexing experiments. From the video, regions of interest within each film were selected and each frame was stitched into a single-row montage in ImageJ. This montage was then compressed in the x-direction for visualization purposes. Average intensity within these regions of interest was also plotted against time and normalized.

Results and discussion

Characterization of ITO films deposited on bare and PDMS-coated glass coverslips

ITO was first deposited on bare and PDMS-coated glass coverslips as a 200 nm thin film using radio frequency sputtering. As shown by the SEM image in Fig. 1Ai, ITO deposited directly on glass coverslips formed a smooth, uniform surface with occasional nanoscale islands, which may have developed due to the migration and accumulation of highly mobile In and Sn atoms. In contrast, ITO deposited on PDMS-coated glass coverslips showed a textured morphology (Fig. 1Aii), likely due to the natural stress relaxation of the deposited ITO film that deformed the underlying viscoelastic PDMS layer. This difference in morphology had a direct consequence on the electrical properties of the ITO films on the two substrates. The measured sheet resistance of ITO on glass coverslips was 302 ± 118 Ω per square (n = 6), whereas that of ITO on PDMS-coated glass coverslips was 400 ± 235 Ω per square (n = 6). We then assessed optical transmittance across the visual spectrum (~400-740 nm) for all conditions, as shown in Fig. 1B. Transmittance for both bare and PDMS-coated glass coverslips without ITO was close to one across the entire spectrum. The ITO coating reduced transmittance for both bare and PDMS-coated glass coverslips due to the additional

reflection and absorption from the ITO layer. As expected, based on the SEM images, transmittance was lower for PDMS-coated glass coverslips coated with ITO compared to bare glass coverslips coated with ITO. However, transmittance was still relatively high across the visible spectrum for all substrates. Thus, bare and PDMS-coated glass coverslips coated with ITO films were both conductive and semi-transparent.

Fabrication of parallel ITO electrodes to stimulate calcium transients

As described above, patterning cardiac tissues to mimic the alignment of native myocardium and subsequently measuring calcium transients are two prioritized features for Heart-on-a-Chip devices. To achieve both features with ITO electrodes integrated into the substrate, we deposited two wide strips of ITO on the edges of PDMS-coated coverslips to serve as parallel electrodes (Fig. 2A). To control the geometry of the ITO, removable adhesive tape was laser-cut with the desired pattern and aligned on a PDMS-coated coverslip (Fig. S1). ITO was then deposited onto the coverslip and the tape mask was removed, leaving two wide regions of ITO on opposing borders of the coverslip (Fig. 2B). Electric field simulations predicted relatively even distribution of voltage between the electrodes (Fig. 2C). We also simulated the electric field generated by an external parallel platinum electrode positioned above a coverslip (Fig. 2C), which resulted in a field distribution with less uniformity than the surface-integrated ITO electrodes. We then microcontact printed arrayed 15-μm lines of fibronectin separated by 2 μm over the entire PDMS-coated coverslip, including regions coated with ITO, and bonded a rectangular PDMS frame on top of the coverslip aligned perpendicular to the parallel electrodes to serve as a cell culture chamber (Fig. 2A).

Next, neonatal rat ventricular myocytes were seeded in the PDMS chamber, which self-assembled into an aligned tissue after three days in culture. Tissue confluence, alignment, and general health were confirmed by brightfield imaging, which was possible in regions with and without ITO coating (Fig. 2D). We then incubated the tissue with Fluo-4, transferred the

device to an inverted fluorescence microscope, and connected the exposed regions of ITO outside of the cell culture chamber to an external stimulator using conductive tape. While pacing the tissue with 20 V at 1.0 Hz, we recorded Fluo-4 fluorescence (Movie S1, Fig. 2E) and subsequently plotted calcium transients in a region of interest (Fig. 2F) using custom MATLAB software.[65] As expected, calcium transients occurred at 1 Hz, matching the stimulation frequency. These data demonstrate that ITO electrodes deposited on PDMS can successfully pace cardiac tissues that are aligned by fibronectin micropatterned on the same continuous PDMS layer.

Fabrication of point ITO electrodes to stimulate calcium wave propagation

Another important physiological metric for assessing engineered cardiac tissues is propagation velocity, which requires a point electrode to stimulate a very small region of the tissue. Voltage and calcium signals then propagate outwards from the initial site of activation, which can be imaged using voltage- or calcium-sensitive dyes, respectively.[13, 14, 19] To stimulate calcium wave propagation with ITO electrodes, we designed a tape mask that included two wide regions of ITO on opposing sides of the coverslip (similar to Fig. 2) and two thin rectangles that extended from these wide regions to the center of the coverslip, where they were separated by a 0.5 mm gap (Fig. 3A). Simulations predicted that this design would generate a highly localized and uniform electric field in the gap between the ITO projections (Fig. 3B) and thus act as a point electrode. Using the same techniques described above, PDMS-coated coverslips were covered with the tape mask during ITO deposition, microcontact printed with fibronectin, and seeded with neonatal rat ventricular myocytes.

After three days in culture, we incubated the micropatterned cardiac tissue with Fluo-4 and imaged it using both brightfield and fluorescence microscopy. Consistent with the analysis shown in Fig. 1, ITO caused some discoloration but did not prevent brightfield imaging (Fig. 3C). In contrast, Fluo-4 fluorescence was almost completely blocked by the

ITO, preventing capture of Fluo-4 signal in the regions deposited with ITO (Fig. 3D). For this reason, we aligned the tissue perpendicular to the ITO point electrodes to maximize the field of view for capturing propagation of the calcium wave in the longitudinal direction of the tissue (Fig. 3C). Longitudinal propagation velocity is faster and more relevant to cardiac tissue physiology compared to the transverse direction.[9, 13] After connecting the exposed regions of ITO to an external stimulator using conductive tape, the tissue was paced at 1.0 Hz and a movie of Fluo-4 fluorescence was captured for 4 s (Movie S2, Fig. 3D). Next, we calculated a map of the maximum change in fluorescence intensity over time for each pixel (Fig. 3E), which is useful for visualizing the calcium wave front and identifying regions that are optimal for measuring calcium wave propagation velocity.[9] The calcium wave originated between the electrodes and traveled with an elliptical wave front, as expected for an aligned cardiac tissue. Next, we cropped the movie to isolate a segment of the wave front that was parallel to the alignment of the tissue to calculate longitudinal propagation velocity (Fig. 3E**)**. After separating each 1 s activation cycle (Fig. 3F), we plotted distance against activation time within the region of interest and quantified the slope of this line as the calcium wave propagation velocity for each activation cycle (Fig. 3G). The values of propagation velocity were similar to those recorded from aligned cardiac tissues stimulated by an external point stimulation electrode.[9] Collectively, these data demonstrate that the point ITO electrode on PDMS effectively stimulated a small region of micropatterned cardiac tissue, inducing calcium waves to propagate outwards and enabling quantification of propagation velocity.

Integration of parallel ITO electrodes into MTF devices to stimulate contraction

The MTF assay was previously developed to measure forces generated by engineered muscle tissues by culturing cells on laser-cut cantilevers of microcontact-printed PDMS, which deflect as the tissues contract.[13, 25, 26] The cantilevers are temporarily adhered to a glass coverslip during cell culture by a sacrificial layer of PIPAAm that is solubilized at the time of

the assay by reducing the temperature. Conventionally, the MTF assay requires a user to manually position a parallel platinum electrode built into a Petri dish over the MTF substrate, which is relatively bulky and limits the user to stimulating all cantilevers at the same frequency. To overcome these limitations, we designed and deposited two sets of parallel ITO electrodes onto glass coverslips using laser-cut tape masks that each encompass a row of MTFs (Fig. 4A and B). Similar to the point electrode pattern, each electrode was connected to a wide region of ITO on the sides of the coverslip for connection to external stimulators. After ITO deposition on the glass coverslip, tape masks were used to sequentially deposit two rectangles of PIPAAm covered by two larger rectangles of PDMS (Fig. 4Ci), which were each positioned inside a set of parallel ITO electrodes. Next, we laser-cut rectangular cantilevers into the PDMS (Fig. 4Cii) and microcontact printed fibronectin in alignment with the length of the MTFs. Finally, a PDMS chamber with a center divider (Fig. 4A, Fig. S3) was bonded to the coverslip to separate each set of MTFs with its corresponding electrodes. Similar to the parallel electrodes for the calcium imaging device (Fig. 2), simulations predicted that this electrode pattern would maintain uniform voltage distribution within each set of ITO electrodes, where the MTFs are located (Fig. 4D). A complete assembled device is shown in Fig. 4E.

Next, neonatal rat ventricular myocytes were seeded and cultured on an ITO MTF device. Cell alignment was confirmed in the direction of the MTF using brightfield imaging **(**Fig. 5A). We then moved the device to a stereomicroscope and added room temperature Tyrode's solution to activate the phase transition of PIPAAm. Upon PIPAAm dissolution, we carefully peeled MTFs from the glass coverslip using tweezers and raised the temperature to 37°C. Similar to the parallel and point electrode experiments, we connected the exposed regions of ITO to conductive tape (Fig. 5B) and external field stimulators (Fig. 5C). Because this device had two PDMS chambers, each with two MTFs, the device was linked to two separate stimulators for independent control of the MTFs in each chamber. Next, we recorded

videos of MTFs in each well while pacing tissues at 0.5, 1.0, and 2.0 Hz. Based on the deflection of the MTFs (Fig. 5D, Movie S3), we calculated contractile stress profiles at each frequency by assuming that the film is a plane strain beam.[13, 25, 26] As shown in Fig. 5E, MTFs contracted in synchrony with each stimulation frequency, indicating successful pacing by the ITO electrodes. Additionally, the MTFs generated stresses on the same order of magnitude as previously reported studies using conventional stimulation electrodes.

To demonstrate that distinct sets of ITO electrodes on the same substrate can stimulate their corresponding MTFs independently, we next set each external field stimulator to pace at different frequencies during a 30 s recording. Starting at 1.0 Hz for the top chamber and 0.5 Hz for the bottom chamber (Fig. 6A, Movie S4), the frequencies were switched approximately every 10 s. As expected, each pair of MTFs contracted at the frequency designated by their respective stimulator. This was confirmed by selecting regions of interest (white squares in Fig. 6A) within each MTF, stitching the images from the video into a single-row montage, and compressing them in the x-direction to easily visualize the physical movement of the MTFs (Fig. 6B). Average pixel intensity within each region of interest was also plotted over time (Fig. 6C). As seen using both methods, each set of MTFs contracted according to its respective stimulation frequency with no interference from the other set. These results demonstrate that patterned ITO electrodes can be used to independently pace different regions of cardiac tissue within a single Heart-on-a-Chip device, which can be implemented to improve multiplexing and ultimately increase throughput.

Conclusions

In this study, we integrated parallel or point electrodes into Heart-on-a-Chip devices featuring tunable culture surfaces and quantitative physiological assays. Electrodes were fabricated from ITO, which is semi-transparent and thus does not interfere with brightfield

microscopy, and were patterned using laser-cut tape masks, a facile method compared to contact photolithography. Depending on assay requirements, ITO electrodes were deposited directly on glass or PDMS and then used to successfully stimulate cardiac tissues either globally or locally to measure three key functional readouts: calcium transient morphology, calcium propagation velocity, and contractile stresses. We also demonstrated that multiple sets of ITO electrodes can be patterned on a single device, enabling users to distinctly stimulate different regions of a substrate simultaneously for multiplexing.

Our approach has several advantages over previous strategies for electrically stimulating cardiac tissues *in vitro*. Compared to inserting external electrodes into the tissue bath, we showed that our ITO electrodes provide a more uniform and reproducible electric field. We also demonstrated that our ITO electrodes can be implemented to stimulate different regions of the same substrate at distinct frequencies, a multiplexing feature not feasible with external electrodes. Surface-integrated electrodes are also more compatible with enclosing tissues into a fluidic device or other enclosed system compared to external electrodes, which is often a desirable design feature for Heart-on-a-Chip systems.[26, 66, 67]

Our approach also offers several advantages compared to conventional microelectrode arrays, which are usually fabricated by depositing patterns of opaque metal on a glass substrate using photolithography. Although contact photolithography is advantageous for achieving spatial resolutions on the order of single micrometers, it is not amenable to rapid prototyping because it is a relatively time-consuming process with a high iteration cost. In this study, we used laser-engraved tape masks to pattern electrodes, which is a more flexible technique that can be rapidly customized by the user. Although the spatial resolution of laser-cut tape masks is limited to several hundred micrometers, we showed that this is adequate for generating parallel and point electrodes for stimulating cardiac tissues globally or locally, respectively, which is sufficient for the majority of Heart-on-a-Chip physiological assays.

Another advantage of our approach is the semi-transparency of ITO. Although ITO was not transparent for fluorescence imaging, it was sufficiently transparent for brightfield imaging, which is useful for evaluating basic phenotypes such as cell adhesion, morphology, and beat rate. The transparency of the electrodes could possibly be further optimized by reducing the radiofrequency sputtering power, introducing oxygen to the gas mixture, or performing post-deposition annealing at high temperatures (700-800°C), which could be done only on glass substrates without PDMS.[68-70] Hydrogenated indium oxide can also be explored as a transparent conductor, as it shows transparencies of ~99% and can be directly deposited on desired samples.[71] Graphene microelectrode arrays on glass have been shown to be transparent for fluorescence imaging,[72] but patterning graphene electrodes requires several intricate steps and the use of multiple high-end tools and high-purity gases. Graphene electrodes also cannot be grown directly on desired substrates and thus must be fabricated separately and then transferred to cell culture substrates.[73] In contrast, ITO can be deposited directly on cell culture substrates using fewer steps with tools that are easily accessible in most academic settings, which reduces variability and increases scalability with the tradeoff of reduced transparency for fluorescence imaging.

Another advantage of our approach is the ability to deposit ITO electrodes directly on PDMS, a very popular substrate for Organ-on-Chip systems because it has tunable rigidity, can be microcontact printed with extracellular matrix proteins to dictate tissue architecture, and is highly compatible with replica molding. Although gold electrodes have been deposited on PDMS,[43-45] gold is completely opaque in the entire visible spectrum, which limits the ability to broadly monitor general cell and tissue health throughout the culture period.

One limitation of our multiplexed device is the need for multiple stimulators. This could be addressed in future iterations by integrating a frequency dividing circuit to enable multiple output frequencies from a single input channel. For example, with a ‘divide-by-2’ frequency divider, the input frequency f_0 could pulse different chambers at f_0 divided by 2, f_0

divided by 4, and so on.[74] This would remove the need for multiple stimulators when stimulating wells at different frequencies, which would likely minimize connection errors and improve device portability and integration into a cell culture incubator.

Collectively, we report a facile approach for integrating semi-transparent electrodes into Heart-on-a-Chip devices that also offer tunable culture surfaces and rigorous physiological assays. This is a unique combination of features and the procedures are overall modular, scalable, and easy to adapt to other systems. For example, we envision that these techniques would be useful for stimulating three-dimensional cardiac or skeletal muscle tissues,[75, 76] tissue explants,[65] or neural organoids.[77] Surface-integrated ITO electrodes could also be implemented to provide continuous electrical cues to cells and tissues during extended culture periods, which has been shown to improve the differentiation of engineered cardiac[61, 78-80] and skeletal muscle[81, 82] constructs. The uniformity of the electric field generated by surface-integrated ITO electrodes compared to external electrodes could be especially important for skeletal muscle tissues, which have a graded response to electrical stimulation[83] and thus often require more voltage control compared to cardiac tissue. We also anticipate that ITO could similarly be patterned directly on other types of materials commonly used for cell culture, such as softer blends of PDMS[8] or polystyrene, and could also be deposited directly on larger slabs of PDMS for easy integration into sealed, continuously perfused microfluidic devices. Although ITO cannot be deposited directly on hydrogels, our masking approach could be implemented to first pattern ITO electrodes on a glass substrate and the attach slabs of hydrogels for cell culture.[11] Previous studies have shown that gelatin hydrogels directly on top of conventional microelectrode arrays are sufficiently conductive to enable electrical communication between the electrodes and cells,[84] which would likely be the case for surface-integrated ITO electrodes as well. ITO stimulation electrodes could also be integrated with electronic components for tissue sensing, such as strain gauges,[33, 34] to reduce the reliance on microscopy and further increase throughput. Thus, the facile and modular

approaches reported here have many diverse applications in microphysiological systems for a broad range of excitable tissues.

Author contributions

J.K.Y., D.S., R.K., and M.L.M. designed the project and drafted the manuscript. J.K.Y. performed experiments and data analysis related to device design and fabrication, contractility assays, and calcium imaging. D.S., J.T., and S.K. performed ITO deposition and characterization studies. A.P.P. assisted with calcium wave propagation velocity and transient data analysis. J.G. assisted with device fabrication. M.L.R., N.C., and N.N.K. assisted with the cell harvest. All authors reviewed the manuscript.

Acknowledgements

This research was funded by the Alfred E. Mann Fellowship in Innovation in Engineering (J.K.Y.), the ARCS Scholarship from the University of Southern California (J.K.Y.), the Annenberg Advanced Endowed Fellowship from the University of Southern California (D.S.), the Provost Fellowship from the University of Southern California (J.T., N.N.K.), the Viterbi Internal Center Incubator and Center for Integrated Electronic and Biological Organisms (CIEBOrg) (M.L.M., R.K.), the National Science Foundation award number 1610604 (R.K.), the American Heart Association Scientist Development Grant 16SDG29950005 (M.L.M.) and Postdoctoral Fellowship 19POST34380814 (M.L.R.), and the Rose Hills Foundation Innovator Grant Program (M.L.M.).

References

1. K. H. Benam, S. Dauth, B. Hassell, A. Herland, A. Jain, K. J. Jang, K. Karalis, H. J. Kim, L. MacQueen, R. Mahmoodian, S. Musah, Y. S. Torisawa, A. D. van der Meer, R. Villenave, M. Yadid, K. K. Parker and D. E. Ingber, *Annu Rev Pathol*, 2015, **10**, 195-262.
2. A. K. Capulli, K. Tian, N. Mehandru, A. Bukhta, S. F. Choudhury, M. Suchyta and K. K. Parker, *Lab Chip*, 2014, **14**, 3181-3186.
3. E. W. Esch, A. Bahinski and D. Huh, *Nat Rev Drug Discov*, 2015, **14**, 248-260.
4. D. Huh, Y.-S. Torisawa, G. A. Hamilton, H. J. Kim and D. E. Ingber, *Lab on a Chip*, 2012, **12**, 2156.
5. S. Ahadian, R. Civitarese, D. Bannerman, M. H. Mohammadi, R. Lu, E. Wang, L. Davenport-Huyer, B. Lai, B. Zhang, Y. Zhao, S. Mandla, A. Korolj and M. Radisic, *Adv Healthc Mater*, 2018, **7**.
6. C. A. Walker and F. G. Spinale, *J Thorac Cardiovasc Surg*, 1999, **118**, 375-382.
7. D. M. Lyra-Leite, A. M. Andres, A. P. Petersen, N. R. Ariyasinghe, N. Cho, J. A. Lee, R. A. Gottlieb and M. L. McCain, *Am J Physiol Heart Circ Physiol*, 2017, **313**, H757-H767.
8. R. N. Palchesko, L. Zhang, Y. Sun and A. W. Feinberg, *PLoS ONE*, 2012, **7**.
9. A. P. Petersen, D. M. Lyra-Leite, N. R. Ariyasinghe, N. Cho, C. M. Goodwin, J. Y. Kim and M. L. McCain, *Cellular and Molecular Bioengineering*, 2018, **11**, 337-352.
10. N. Annabi, K. Tsang, S. M. Mithieux, M. Nikkhah, A. Ameri, A. Khademhosseini and A. S. Weiss, *Adv Funct Mater*, 2013, **23**.
11. M. L. McCain, A. Agarwal, H. W. Nesmith, A. P. Nesmith and K. K. Parker, *Biomaterials*, 2014, **35**, 5462--5471.
12. N. R. Ariyasinghe, C. H. Reck, A. A. Viscio, A. P. Petersen, D. M. Lyra-Leite, N. Cho and M. L. McCain, *Integr Biol (Camb)*, 2017, **9**, 730-741.
13. A. W. Feinberg, P. W. Alford, H. Jin, C. M. Ripplinger, A. A. Werdich, S. P. Sheehy, A. Grosberg and K. K. Parker, *Biomaterials*, 2012, **33**, 5732-5741.
14. N. Bursac, K. K. Parker, S. Iravanian and L. Tung, *Circ Res*, 2002, **91**, e45-54.
15. D. H. Kim, E. A. Lipke, P. Kim, R. Cheong, S. Thompson, M. Delannoy, K. Y. Suh, L. Tung and A. Levchenko, *Proc Natl Acad Sci U S A*, 2010, **107**, 565-570.
16. A. Agarwal, Y. Farouz, A. P. Nesmith, L. F. Deravi, M. L. McCain and K. K. Parker, *Adv Funct Mater*, 2013, **23**, 3738-3746.
17. M. L. McCain, S. P. Sheehy, A. Grosberg, J. A. Goss and K. K. Parker, *Proc Natl Acad Sci U S A*, 2013, **110**, 9770-9775.
18. C. I. Spencer, S. Baba, K. Nakamura, E. A. Hua, M. A. Sears, C. C. Fu, J. Zhang, S. Balijepalli, K. Tomoda, Y. Hayashi, P. Lizarraga, J. Wojciak, M. M. Scheinman, K. Aalto-Setälä, J. C. Makielski, C. T. January, K. E. Healy, T. J. Kamp, S. Yamanaka and B. R. Conklin, *Stem Cell Reports*, 2014, **3**, 269-281.
19. A. P. Petersen, N. Cho, D. M. Lyra-Leite, J. W. Santoso, D. Gupta, N. R. Ariyasinghe and M. L. McCain, *Integr Biol (Camb)*, 2020, **12**, 34-46.
20. W. Bian, C. P. Jackman and N. Bursac, *Biofabrication*, 2014, **6**, 024109-024109.
21. Z. Ma, N. Huebsch, S. Koo, M. A. Mandegar, B. Siemons, S. Boggess, B. R. Conklin, C. P. Grigoropoulos and K. E. Healy, *Nat Biomed Eng*, 2018, **2**, 955-967.
22. N. Huebsch, P. Loskill, M. A. Mandegar, N. C. Marks, A. S. Sheehan, Z. Ma, A. Mathur, T. N. Nguyen, J. C. Yoo, L. M. Judge, C. I. Spencer, A. C. Chukka, C. R. Russell, P. L. So, B. R. Conklin and K. E. Healy, *Tissue Eng Part C Methods*, 2015, **21**, 467-479.
23. C. P. Jackman, A. L. Carlson and N. Bursac, *Biomaterials*, 2016, **111**, 66-79.

24. A. W. Feinberg, A. Feigel, S. S. Shevkoplyas, S. Sheehy, G. M. Whitesides and K. K. Parker, *Science*, 2007, **317**, 1366-1370.
25. A. Grosberg, P. W. Alford, M. L. McCain and K. K. Parker, *Lab Chip*, 2011, **11**, 4165-4173.
26. A. Agarwal, J. A. Goss, A. Cho, M. L. McCain and K. K. Parker, *Lab Chip*, 2013, **13**, 3599-3608.
27. A. J. Ribeiro, Y. S. Ang, J. D. Fu, R. N. Rivas, T. M. Mohamed, G. C. Higgs, D. Srivastava and B. L. Pruitt, *Proc Natl Acad Sci U S A*, 2015, **112**, 12705-12710.
28. A. J. Engler, C. Carag-Krieger, C. P. Johnson, M. Raab, H. Y. Tang, D. W. Speicher, J. W. Sanger, J. M. Sanger and D. E. Discher, *J Cell Sci*, 2008, **121**, 3794-3802.
29. M. L. McCain, H. Yuan, F. S. Pasqualini, P. H. Campbell and K. K. Parker, *Am J Physiol Heart Circ Physiol*, 2014, **306**, H1525-1539.
30. M. Radisic, H. Park, H. Shing, T. Consi, F. J. Schoen, R. Langer, L. E. Freed and G. Vunjak-Novakovic, *Proc Natl Acad Sci U S A*, 2004, **101**, 18129-18134.
31. N. Tandon, C. Cannizzaro, P. H. Chao, R. Maidhof, A. Marsano, H. T. Au, M. Radisic and G. Vunjak-Novakovic, *Nat Protoc*, 2009, **4**, 155-173.
32. Y. Zhao, E. Y. Wang, L. H. Davenport, Y. Liao, K. Yeager, G. Vunjak-Novakovic, M. Radisic and B. Zhang, *Adv Healthc Mater*, 2019, **8**, e1801187.
33. J. U. Lind, M. Yadid, I. Perkins, B. B. O'Connor, F. Eweje, C. O. Chantre, M. A. Hemphill, H. Yuan, P. H. Campbell, J. J. Vlassak and K. K. Parker, *Lab Chip*, 2017, **17**, 3692-3703.
34. J. U. Lind, T. A. Busbee, A. D. Valentine, F. S. Pasqualini, H. Yuan, M. Yadid, S.-J. Park, A. Kotikian, A. P. Nesmith, P. H. Campbell, J. J. Vlassak, J. A. Lewis and K. K. Parker, *Nature Materials*, 2016, **1**, 1-7.
35. A. Stett, U. Egert, E. Guenther, F. Hofmann, T. Meyer, W. Nisch and H. Haemmerle, *Anal Bioanal Chem*, 2003, **377**, 486-495.
36. M. Halbach, U. Egert, J. Hescheler and K. Banach, *Cell Physiol Biochem*, 2003, **13**, 271-284.
37. O. Caspi, I. Itzhaki, I. Kehat, A. Gepstein, G. Arbel, I. Huber, J. Satin and L. Gepstein, *Stem Cells Dev*, 2009, **18**, 161-172.
38. A. Natarajan, M. Stancescu, V. Dhir, C. Armstrong, F. Sommerhage, J. J. Hickman and P. Molnar, *Biomaterials*, 2011, **32**, 4267-4274.
39. M. Stancescu, P. Molnar, C. W. McAleer, W. McLamb, C. J. Long, C. Oleaga, J. M. Prot and J. J. Hickman, *Biomaterials*, 2015, **60**, 20-30.
40. M. C. Denyer, M. Riehle, S. T. Britland and A. Offenhauser, *Med Biol Eng Comput*, 1998, **36**, 638-644.
41. J. S. Park, S. I. Grijalva, M. K. Aziz, T. Chi, S. Li, M. N. Sayegh, A. Wang, H. C. Cho and H. Wang, *Lab Chip*, 2018, **18**, 3037-3050.
42. Y. Nam and B. C. Wheeler, *Crit Rev Biomed Eng*, 2011, **39**, 45-61.
43. T. Adrega and S. P. Lacour, *Journal of Micromechanics and Microengineering*, 2010, **20**, 8.
44. O. Akogwu, D. Kwabi, S. Midturi, M. Eleruja, B. Babatope and W. O. Soboyejo, *Materials Science and Engineering B-Advanced Functional Solid-State Materials*, 2010, **170**, 32-40.
45. J. Tang, H. Guo, M. M. Zhao, J. T. Yang, D. Tsoukalas, B. Z. Zhang, J. Liu, C. Y. Xue and W. D. Zhang, *Scientific Reports*, 2015, **5**, 9.
46. V. K. Jain and A. P. Kulshreshtha, *Solar Energy Materials*, 1981, **4**, 151-158.
47. D. E. Carlson and C. R. Wronski, *Applied Physics Letters*, 1976, **28**, 671-673.
48. N. Shibayama, S. Fukumoto, H. Sugita, H. Kanda and S. Ito, *Materials Research Bulletin*, 2018, **106**, 433-438.
49. G. Yu, K. Pakbaz and A. J. Heeger, *Applied Physics Letters*, 1994, **64**, 3422-3424.

50. W. A. Wohlmuth, J. W. Seo, P. Fay, C. Caneau and I. Adesida, *IEEE Photonics Technology Letters*, 1997, **9**, 1388-1390.
51. G. P. Crawford, *Flexible flat panel display technology*, Wiley Online Library, 2005.
52. U. Betz, M. K. Olsson, J. Marthy, M. F. Escolá and F. Atamny, *Surface and Coatings Technology*, 2006, **200**, 5751-5759.
53. N. Rushe, M. Ball, W. M. Carroll, S. Healy, J. McManus and D. Cunningham, *J Mater Sci Mater Med*, 2005, **16**, 247-252.
54. L. H. Raptis, H. L. Brownell, K. L. Firth and L. W. Mackenzie, *DNA Cell Biol*, 1994, **13**, 963-975.
55. L. Raptis, H. L. Brownell, A. M. Vultur, G. M. Ross, E. Tremblay and B. E. Elliott, *Cell Growth Differ*, 2000, **11**, 293-303.
56. Y. Nashimoto, Y. Takahashi, T. Yamakawa, Y. S. Torisawa, T. Yasukawa, T. Ito-Sasaki, M. Yokoo, H. Abe, H. Shiku, H. Kambara and T. Matsue, *Anal Chem*, 2007, **79**, 6823-6830.
57. C. K. Choi, A. E. English, S. I. Jun, K. D. Kihm and P. D. Rack, *Biosens Bioelectron*, 2007, **22**, 2585-2590.
58. M. Guo, J. Chen, X. Yun, K. Chen, L. Nie and S. Yao, *Biochim Biophys Acta*, 2006, **1760**, 432-439.
59. G. W. Gross, B. K. Rhoades, D. L. Reust and F. U. Schwalm, *J Neurosci Methods*, 1993, **50**, 131-143.
60. G. W. Gross, W. Y. Wen and J. W. Lin, *J Neurosci Methods*, 1985, **15**, 243-252.
61. N. Tandon, A. Marsano, R. Maidhof, K. Numata, C. Montouri-Sorrentino, C. Cannizzaro, J. Voldman and G. Vunjak-Novakovic, *Lab Chip*, 2010, **10**, 692-700.
62. T. A. König, P. A. Ledin, J. Kerszulis, M. A. Mahmoud, M. A. El-Sayed, J. R. Reynolds and V. V. Tsukruk, *ACS Nano*, 2014, **8**, 6182-6192.
63. Y. Huang, X. B. Wang, F. F. Becker and P. R. Gascoyne, *Biophys J*, 1997, **73**, 1118-1129.
64. D. Qin, Y. Xia and G. M. Whitesides, *Nat Protoc*, 2010, **5**, 491-502.
65. J. K. Yip, M. Harrison, J. Villafuerte, G. E. Fernandez, A. P. Petersen, C. L. Lien and M. L. McCain, *Lab Chip*, 2020, **20**, 274-284.
66. B. M. Maoz, A. Herland, O. Y. F. Henry, W. D. Leineweber, M. Yadid, J. Doyle, R. Mannix, V. J. Kujala, E. A. FitzGerald, K. K. Parker and D. E. Ingber, *Lab Chip*, 2017, **17**, 2294-2302.
67. A. Mathur, P. Loskill, K. Shao, N. Huebsch, S. Hong, S. G. Marcus, N. Marks, M. Mandegar, B. R. Conklin, L. P. Lee and K. E. Healy, *Sci Rep*, 2015, **5**, 8883.
68. F. Kurdesau, G. Khripunov, A. da Cunha, M. Kaelin and A. Tiwari, *Journal of Non-Crystalline Solids*, 2006, **352**, 1466-1470.
69. A. Ali, Z. Hassan and A. Shuhaimi, *Applied Surface Science*, 2018, **443**, 544-547.
70. C. Guillen and J. Herrero, *Thin Solid Films*, 2005, **480**, 129-132.
71. C. Battaglia, L. Erni, M. Boccard, L. Barraud, J. Escarre, K. Soderstrom, G. Bugnon, A. Billet, L. Ding, M. Despeisse, F. Haug, S. De Wolf and C. Ballif, *Journal of Applied Physics*, 2011, **109**.
72. S. K. Rastogi, J. Bliley, D. J. Shiwarski, G. Raghavan, A. W. Feinberg and T. Cohen-Karni, *Cell Mol Bioeng*, 2018, **11**, 407-418.
73. X. Li, W. Cai, J. An, S. Kim, J. Nah, D. Yang, R. Piner, A. Velamakanni, I. Jung, E. Tutuc, S. Banerjee, L. Colombo and R. Ruoff, *Science*, 2009, **324**, 1312-1314.
74. G. M. Xiong, A. T. Do, J. K. Wang, C. L. Yeoh, K. S. Yeo and C. Choong, *J Biol Eng*, 2015, **9**, 14.
75. Y. Xiao, B. Zhang, H. Liu, J. W. Miklas, M. Gagliardi, A. Pahnke, N. Thavandiran, Y. Sun, C. Simmons, G. Keller and M. Radisic, *Lab Chip*, 2014, **14**, 869-882.

76. L. Madden, M. Juhas, W. E. Kraus, G. A. Truskey and N. Bursac, *Elife*, 2015, **4**, e04885.
77. G. Quadrato and P. Arlotta, *Curr Opin Cell Biol*, 2017, **49**, 47-52.
78. Y. Ganji, Q. Li, E. S. Quabius, M. Böttner, C. Selhuber-Unkel and M. Kasra, *Mater Sci Eng C Mater Biol Appl*, 2016, **59**, 10-18.
79. K. Ronaldson-Bouchard, S. P. Ma, K. Yeager, T. Chen, L. Song, D. Sirabella, K. Morikawa, D. Teles, M. Yazawa and G. Vunjak-Novakovic, *Nature*, 2018, **556**, 239-243.
80. L. L. Chiu, R. K. Iyer, J. P. King and M. Radisic, *Tissue Eng Part A*, 2011, **17**, 1465-1477.
81. A. Ito, Y. Yamamoto, M. Sato, K. Ikeda, M. Yamamoto, H. Fujita, E. Nagamori, Y. Kawabe and M. Kamihira, *Sci Rep*, 2014, **4**, 4781.
82. T. Nedachi, H. Fujita and M. Kanzaki, *Am J Physiol Endocrinol Metab*, 2008, **295**, E1191-1204.
83. F. Cao, C. Zhang, T. T. Vo Doan, Y. Li, D. H. Sangi, J. S. Koh, N. A. Huynh, M. F. Bin Aziz, H. Y. Choo, K. Ikeda, P. Abbeel, M. M. Maharbiz and H. Sato, *PLoS One*, 2014, **9**, e105389.
84. V. J. Kujala, F. S. Pasqualini, J. A. Goss, J. C. Nawroth and K. K. Parker, *Journal of Materials Chemistry B*, 2016, **4**, 3534-3543.

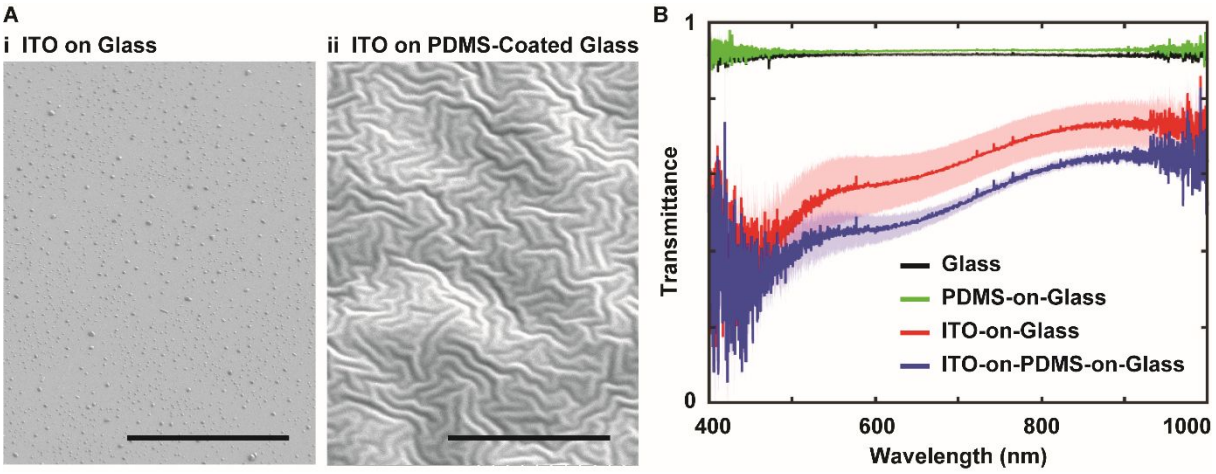

Fig. 1 Surface morphology and transmittance of bare and PDMS-coated glass coverslips coated with ITO. A) Scanning electron microscopy images of (i) ITO on a glass coverslip and (ii) ITO on a PDMS-coated glass coverslip. Scale bars: 10 μm. B) Transmittance measurements of substrates across the visual spectrum. Data presented as mean ± standard deviation (n = 5 for Glass and PDMS-on-Glass, n = 9 for ITO-on-Glass and ITO-on-PDMS-on-Glass).

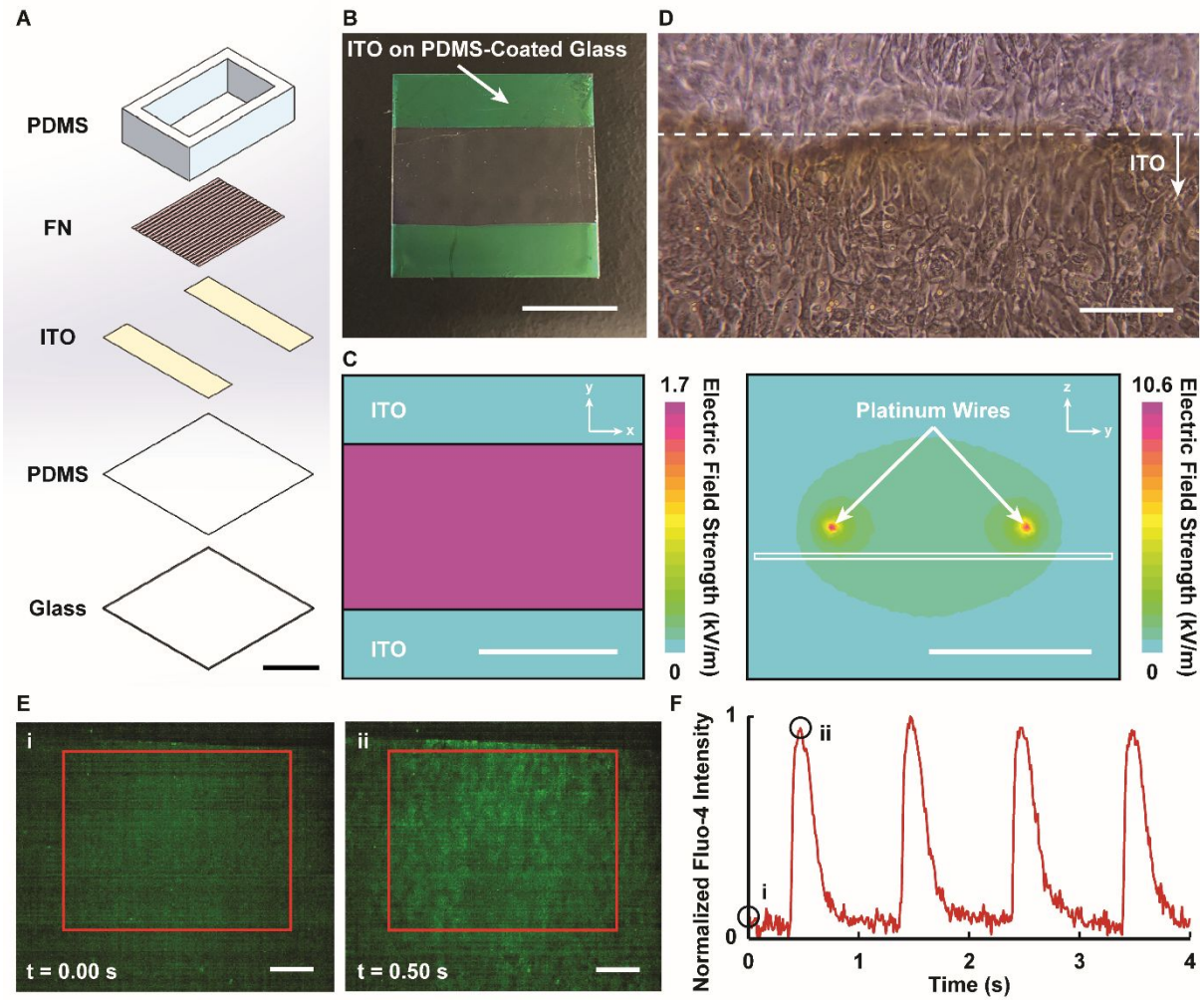

Fig. 2 Fabricating parallel ITO electrodes on PDMS-coated coverslips to stimulate calcium transients in micropatterned cardiac tissues. A) Schematic of device, consisting of a glass coverslip, a spin-coated layer of PDMS, a patterned layer of ITO, microcontact printed fibronectin (FN), and a PDMS cell culture chamber. B) Photograph of parallel ITO electrodes on a PDMS-coated coverslip. C) Left, simulated electric field profile (top view) of the ITO parallel electrodes with an applied voltage of 20 V. Right, simulated electric field profile (side view) of external platinum parallel electrodes with an applied voltage of 20 V. The outlined rectangle represents the typical location of a coverslip, roughly 2 mm below the wires. D) Brightfield image of micropatterned neonatal rat ventricular myocytes three days after seeding. The cells form a monolayer that spans the ITO film on the PDMS-coated coverslip, which is located below the dotted line. E) Fluorescent images of tissue incubated with Fluo-4 and paced at 1.0 Hz and 20 V with parallel ITO electrodes. Frames show the tissue at the beginning of the activation cycle (i) and at peak intensity (ii). F) Average Fluo-4 signal (normalized) for the region of interest indicated in E. The circled time points correspond to sub-panels Ei and Eii. Scale bars: 10 mm for A, B, and C; 100 μm for D; 1 mm for E.

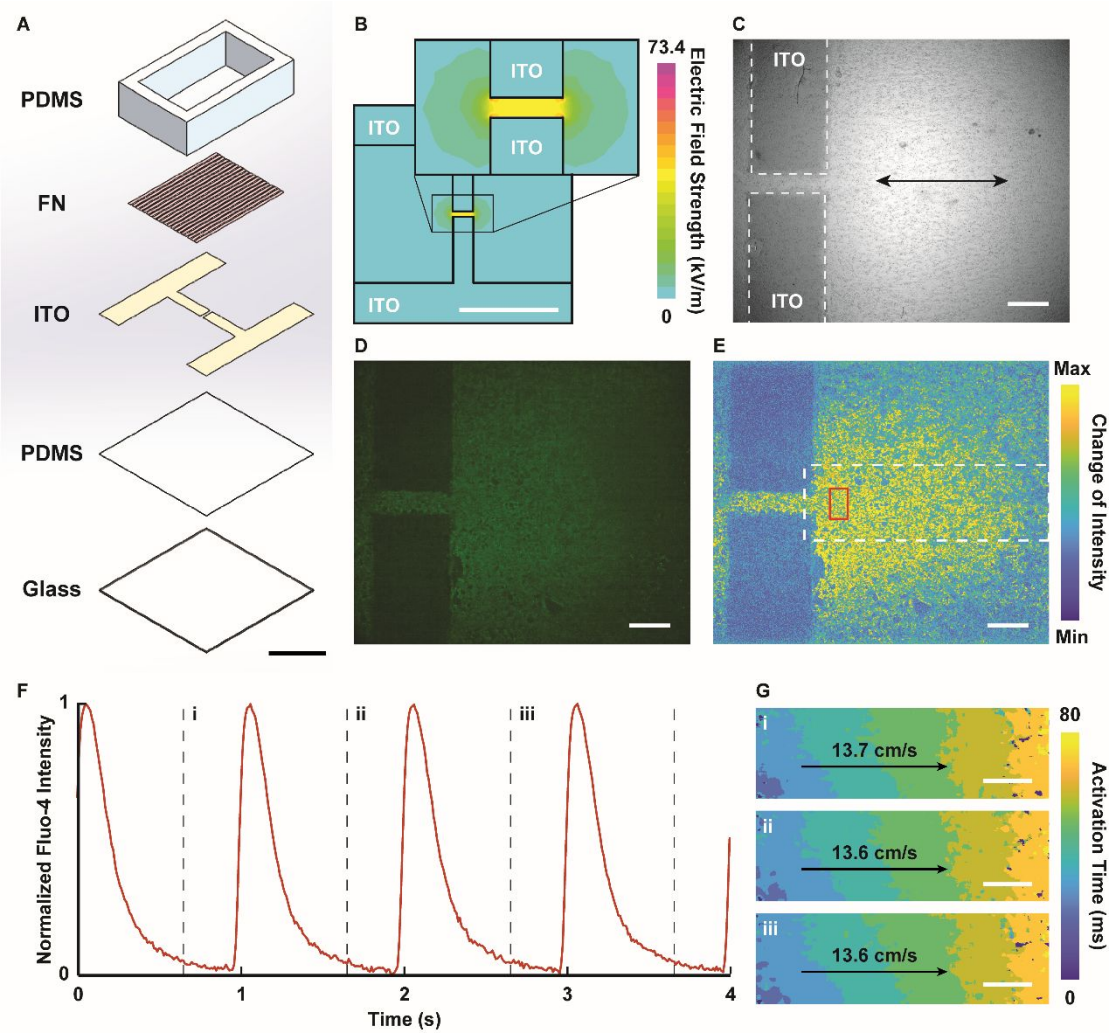

Fig. 3 Fabricating point ITO electrodes on PDMS-coated coverslips to stimulate calcium wave propagation in micropatterned cardiac tissues. A) Schematic of device, consisting of a glass coverslip, a spin-coated layer of PDMS, a patterned layer of ITO, microcontact printed fibronectin (FN), and a PDMS cell culture chamber. B) Simulated electric field profile of the ITO point electrodes with an applied voltage of 20 V. Inset shows the area between the point electrodes in more detail. C) Brightfield image of aligned cardiac tissue cultured on device for three days. The double-headed arrow indicates direction of alignment. D) Fluorescent image of an aligned cardiac tissue incubated with Fluo-4 and paced at 1.0 Hz and 20 V with a point ITO electrode. E) Change of fluorescent intensity of each pixel across a 4 s video. Regions of interest (red, dashed white lines) were used for further analysis. F) Representative calcium transient from the red region of interest in E. Automatic peak detection divided the signal into activation cycles, separated by the dotted lines and labelled i-iii. G) For each of the three activation cycles in F, a corresponding activation map (i-iii) was generated for the white region of interest in E. The calcium wave propagation velocity is shown above the arrow,

which indicates the direction of the wave. Scale bars: 10 mm for A and B; 1 mm for C, D, E, and G.

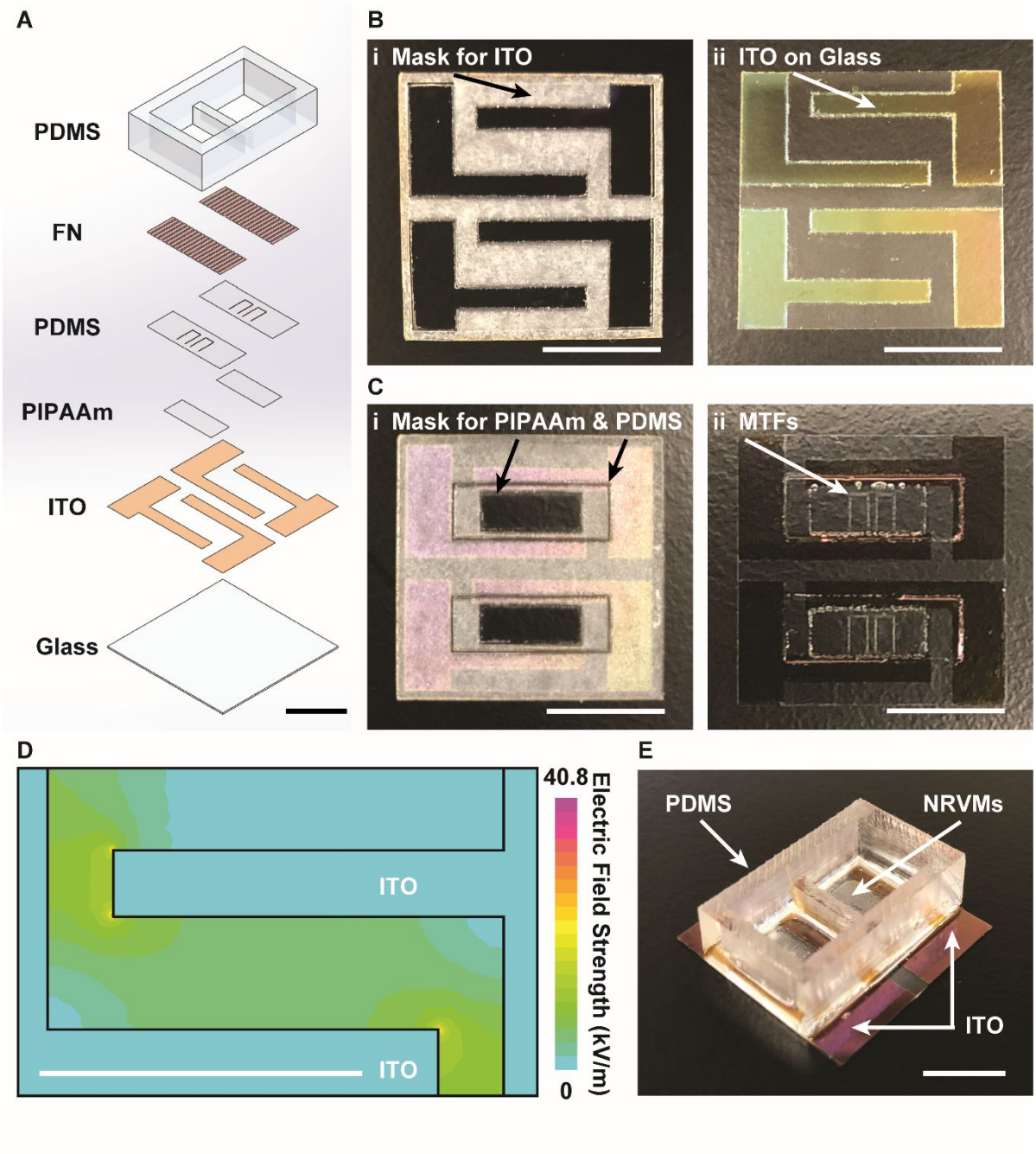

Fig. 4 Fabricating parallel ITO electrodes on MTF devices to stimulate contraction of micropatterned cardiac tissues. A) Schematic of device, consisting of a glass coverslip, a patterned layer of ITO, spin-coated layers of PIPAAm and PDMS, microcontact printed fibronectin (FN), and a PDMS cell culture chamber with a divider splitting the device into two wells. B) Photographs of a coverslip (i) with a tape mask and (ii) after ITO deposition. C) Photographs of a coverslip with (i) a tape mask for PIPAAm and PDMS and (ii) laser-cut MTF cantilevers. D) Simulated electric field profile of one of the pairs of ITO parallel

electrodes with an applied voltage of 20 V. E) Photograph of a complete assembled device. Scale bars: 10 mm.

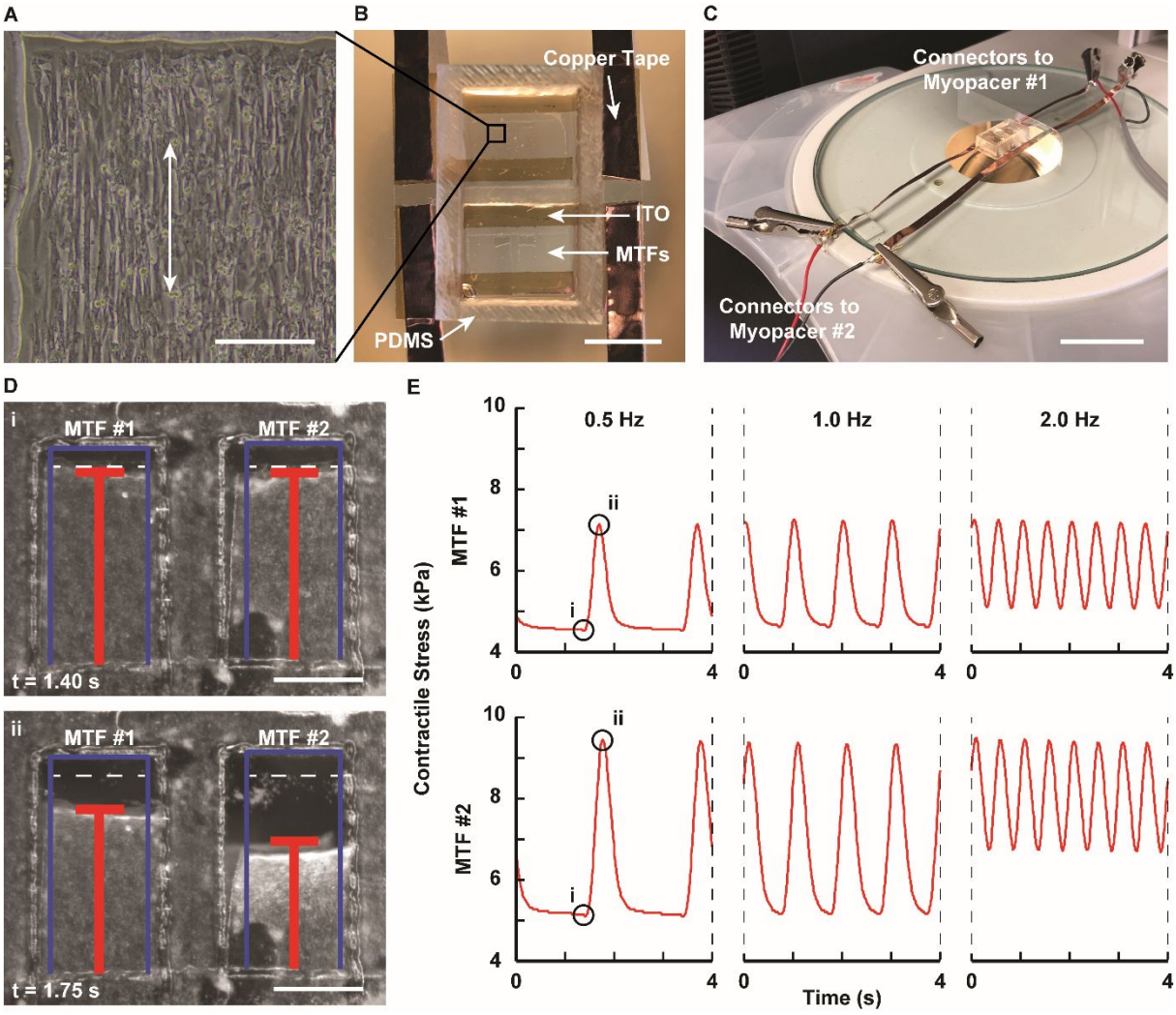

Fig. 5 Measuring contractile stresses generated by MTFs stimulated by parallel ITO electrodes. A) Brightfield image of aligned cardiac tissue on MTF cantilever three days after seeding. The double-headed arrow indicates direction of alignment. B) Photograph of contractility device showing MTFs and connections between ITO and conductive copper tape. C) Photograph of device during assay. The tape electrically connects each pair of ITO electrodes to external field stimulators (Myopacers). D) Frames of MTFs stimulated at 0.5 Hz and 20 V from diastole (i) to peak systole (ii). Blue boxes indicate lengths of MTFs prior to peeling from base substrate. Red "T" bars indicate the horizontal projection tracking of each MTF. E) Representative traces of contractile stress generated from the MTFs in D at indicated pacing frequencies. The circled time points correspond to Di and Dii. Scale bars: 100 μm for A; 10 mm for B; 50 mm for C; 1 mm for D.

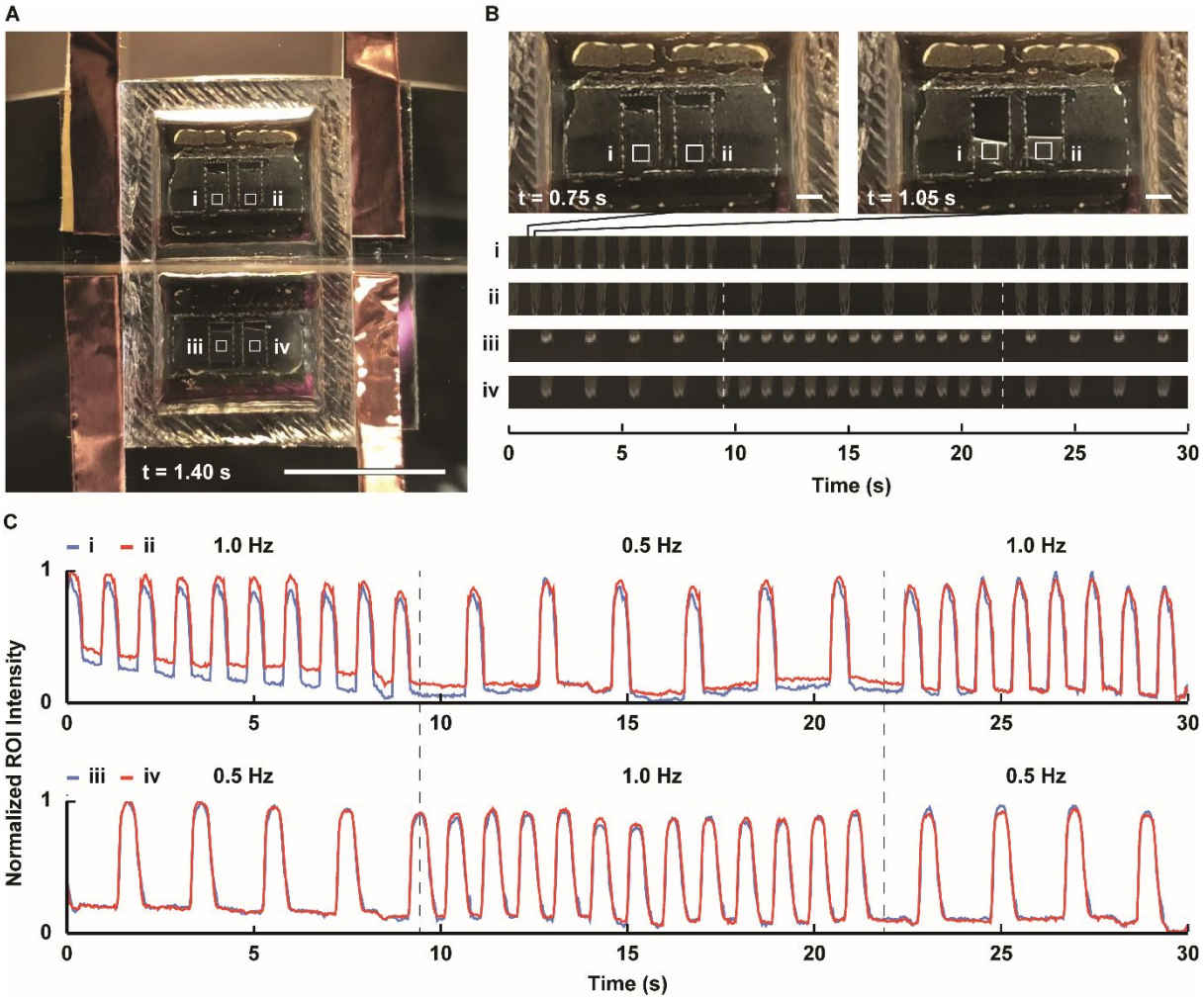

Fig. 6 Independent stimulation of two sets of MTFs within a single device. A) Brightfield image of MTFs in two compartments separated by the PDMS chamber. White squares (i-iv) indicate regions of interest for further analyses. Scale bar: 10 mm. B) Montages of regions of interest from Ai-iv. 925 frames from brightfield videos of each region of interest were stitched together in a single row montage and compressed in the x-direction to display the movement of each MTF over time. Insets show MTFs within the top chamber at diastole, when the regions of interest appear darker, to peak systole, when they appear lighter. These correspond to the black and grey regions in the compressed montages. C) Representative traces of MTFs (normalized intensity of Ai-iv across 30 s) paced at 1.0 Hz (Ai-ii) and 0.5 Hz (Aiii-iv) at 20 V. Approximately every 10 s, the stimulation frequencies were switched to the indicated values.